

Dynamics of two particles with quasiperiodic long-range interactions

Yun Zou^{1,*}

¹*School of Physics and Astronomy, Yunnan Key Laboratory for Quantum Information, Yunnan University, Kunming 650091, PR China*

We investigate the dynamics of two identical spinless fermions on a one-dimensional lattice with open boundary conditions (OBC), subject to quasiperiodic long-range interactions. Using numerical exact diagonalization (ED), we study this non-integrable system as a continuous-time quantum walk and uncover a robust correlated dynamical regime. This regime, characterized by an approximately constant inter-particle distance, emerges under sufficiently strong quasiperiodic modulation of the long-range interactions. Further, the study shows that the behavior is determined by the nature of the interaction and the choice of boundary condition. Notably, by tuning the phase of the quasiperiodic modulation, we observe three distinct manifestations of this phenomenon: localization, nearest-neighbor separation oscillations, and next-nearest-neighbor separation transitions—each arising for specific initial separations. Furthermore, we identify the suppression of entanglement entropy in the system, including instances of oscillatory behavior. Our results highlight how quasiperiodic long-range interactions shape few-body quantum dynamics.

Introduction- Advances in quantum simulator technologies in recent years enable direct investigation of nonequilibrium dynamics in complex systems through precise Hamiltonian engineering. These quantum platforms allow continuous tuning of interaction parameters in the effective model, making the observation of resulting dynamics possible. Furthermore, their strong isolation from external noise supports long-lasting coherent dynamics in the simulated system [1]. This has prompted an investigation into the dynamics of isolated complex systems—a topic of significant interest in theoretical physics, whose answer promises to boost developments in quantum technology [2].

The tunability of current quantum simulators allows for custom-designed interactions, fueling extensive research into the long-range interacting quantum systems [3], which are more complex than short-range systems. Conventionally, the term “long-range” refers to interactions decaying as $1/r^\alpha$ with distance r between particles in an interacting quantum system. However, long-range interactions can also take other forms, such as the quasiperiodically modulated ones considered in this work. Long-range quantum systems are realized in various experimental platforms, such as Rydberg atom arrays [4], dipolar systems [5, 6], trapped ions setups [7], and cold atoms in cavity experiments [8–10], making them promising candidates for building efficient quantum computing devices [11].

The non-interacting quasiperiodic model, best known in one dimension as the Aubry-André model [12], has been studied for decades and has been experimentally realized in ultracold atomic systems via on-site quasiperiodic potentials [13]. However, research into models where the interactions themselves are quasiperiodic, particularly in long-range systems, is a very recent development.

In this work, we investigate the dynamics of two identical spinless fermions on a one-dimensional lattice with open boundary conditions (OBC), subject to quasiperi-

odic long-range interactions. When interactions are sufficiently strong, we uncover a correlated dynamical regime characterized by two particles walking together while maintaining an approximately constant inter-particle distance. This behavior persists across all phases of the quasiperiodic modulation. Tuning the phase reveals three distinct manifestations of this phenomenon, which we discuss as representative examples:

1. sustained localization of both particles under specific conditions;
2. nearest-neighbor separation oscillations of both particles under certain conditions;
3. next-nearest-neighbor separation transitions only under a narrow range of conditions.

Furthermore, we identify the suppression of entanglement entropy in the system, including instances of oscillatory behavior.

We consider fermions in a lattice with quasiperiodic long-range interaction,

$$\hat{H} = -J \sum_{i=1}^L (\hat{c}_i^\dagger \hat{c}_{i+1} + \text{H.c.}) + \sum_{1 \leq i < j \leq L} \Delta \cos(2\pi\beta|i-j| + \varphi) \hat{n}_i \hat{n}_j. \quad (1)$$

Here, \hat{c}_i^\dagger (\hat{c}_i) and $\hat{n}_i = \hat{c}_i^\dagger \hat{c}_i$ are the operators of fermionic creation (annihilation) and particle number at the i th site, respectively. The system size is L . J denotes the nearest-neighbor hopping strength. The interaction term $U = \sum_{1 \leq i < j \leq L} U_{ij}$, with $U_{ij} = \Delta \cos(2\pi\beta|i-j| + \varphi) \hat{n}_i \hat{n}_j$ describes a quasiperiodically modulated long-range interaction between a pair of sites (i, j) , where Δ , β , and φ represent the modulation amplitude, spatial frequency, and initial phase, respectively. The interaction strength varies with the inter-site

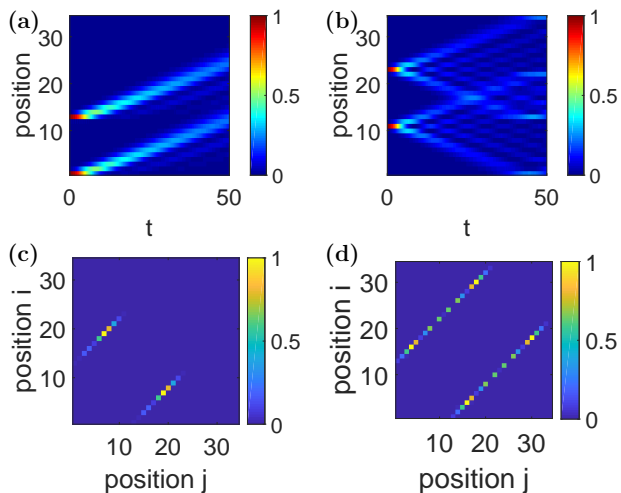


FIG. 1. Probability density evolution and two-particle correlations. (a, b) Probability density $P(i, t)$ [defined in Eq. (2)] up to time $t = 50$ for an initial inter-particle distance of 12, with (a) one particle initially at the boundary and (b) both particles away from the boundary. (c, d) Corresponding two-particle correlation functions $\Gamma(i, j)$ [defined in Eq. (3)] at $t = 30$ for the same initial configurations as (a) and (b), respectively. $L = 34$, $\Delta = 10$, $\varphi = 0$.

distance $r = |i - j|$ in a cosine form with spatial period controlled by the dimensionless parameter β (chosen as an irrational number to realize quasiperiodicity). This model can be effectively realized in experimental platforms such as superconducting circuits [14] and ultracold atoms [15, 16] by mapping its low-dimensional, complex interaction profiles onto an experimentally feasible higher-dimensional synthetic lattice system, where the interactions are effectively represented as simple on-site potentials [17].

Our study focuses on a continuous-time quantum walk of two interacting particles, by concentrating on the strong-interaction regime and, without loss of generality, setting $J = 1$ and $\beta = (\sqrt{5} - 1)/2$. We observe that two identical spinless fermions, subject to quasiperiodic long-range interactions on a one-dimensional lattice with open boundary conditions (OBC), maintain an approximately constant inter-particle distance during their quantum walk, regardless of their initial separation and whether one or both particles start from the boundaries; see Fig. 1.

Under these conditions and for strong interactions ($\Delta = 10$), Figs. 1(a) and (b) display the evolution of the single-particle probability density distribution [18, 19]:

$$P(i, t) = \langle \Psi(t) | \hat{n}_i | \Psi(t) \rangle. \quad (2)$$

This quantity represents the probability of finding a particle at site i at time t . The evolution is shown up to time $t = 50$. In Fig. 1(a), when one particle is initially placed at the boundary, the pair is observed to walk predominantly in one direction, with the inter-particle distance

remaining approximately constant over an extended period; in Fig. 1(b) where both particles start away from the boundaries, the walk occurs symmetrically in two directions, making the constant-distance behavior less visually prominent.

As a complementary view, Figs. 1(c) and (d) show the two-particle correlation function at a fixed time $t = 30$. The correlation function is defined as

$$\Gamma(i, j, t) = \langle \Psi(t) | \hat{c}_i^\dagger \hat{c}_j^\dagger \hat{c}_j \hat{c}_i | \Psi(t) \rangle, \quad i \neq j, \quad (3)$$

which quantifies the joint probability of finding one particle at site i and the other at site j [18, 19]. For identical fermions, the Pauli exclusion principle ensures $\Gamma(i, i, t) = 0$, and the distribution is symmetric, $\Gamma(i, j, t) = \Gamma(j, i, t)$. These correlations reveal that, regardless of whether a particle starts at the boundary or not, the two particles maintain a nearly fixed separation, highlighting a coordinated, pair-like walking mode.

Let us now turn to a discussion of the effects of the interaction strength Δ , presented in Fig. 2. We consider a lattice of size $L = 34$. Eight representative initial positions of the two particles were selected: (1, 2), (1, 34), (1, 17), (5, 15), (10, 25), (8, 26), (3, 31), (15, 20). These configurations cover a range of inter-particle distances, including cases where both particles are on the same boundary, on opposite boundaries, one on a boundary and one in the interior, or both in the interior.

The expected inter-particle distance,

$$\langle r(t) \rangle = \sum_{i < j} |i - j| |\psi_{ij}(t)|^2, \quad (4)$$

where $\psi_{ij}(t) = \langle i, j | \Psi(t) \rangle$, is shown in Figs. 2(a) and (b) up to $t = 300$ for weak ($\Delta = 1$) and strong ($\Delta = 10$) interaction regimes, respectively. Under weak interactions, the expected distance $\langle r(t) \rangle$ fluctuates randomly without a discernible pattern. In contrast, under strong interactions, $\langle r(t) \rangle$ remains close to the initial inter-particle distance $|i_0 - j_0|$, suggesting the two particles form a long-lived, loosely bound pair—that is, a correlated pair whose relative motion is confined by their quasiperiodic interactions.

Fig. 2(c) plots the expected distance $\langle r \rangle$ as a function of the interaction strength Δ at a fixed time $t = 10$. Across all eight configurations, $\langle r \rangle$ is further stabilized and becomes well-defined as Δ increases. We therefore define a characteristic interaction strength $\Delta_0 = 7.58$ from the point in Fig. 2(d) where the variance,

$$\sigma^2 = \sum_{i < j} |i - j|^2 |\psi_{ij}|^2 - \left(\sum_{i < j} |i - j| |\psi_{ij}|^2 \right)^2, \quad (5)$$

across the eight configurations falls below 0.50.

The two particles maintain approximately constant separation during their walk due to the quasiperiodic

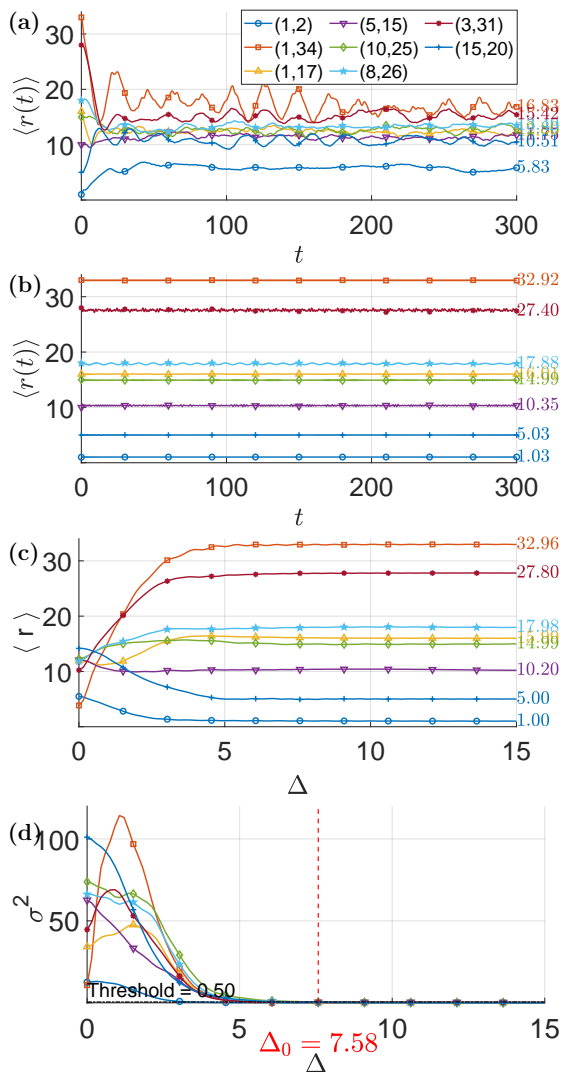


FIG. 2. Expected inter-particle distance and its variance. (a,b) Time evolution of the expected inter-particle distance $\langle r(t) \rangle$ [defined in Eq. (4)] up to $t = 300$ for (a) $\Delta = 1$ and (b) $\Delta = 10$. (c,d) At $t = 10$: (c) expected distance $\langle r \rangle$ and (d) variance [defined in Eq. (5)] as a function of Δ . Dashed line in (d): variance threshold $0.50 \rightarrow \Delta_0 = 7.58$. $L = 34$, $\varphi = 0$.

modulation described by the Hamiltonian \hat{H} in Eq.(1). As the inter-particle distance $r = |i - j|$ changes by one lattice unit, the modulation term U_{ij} exhibits a roughly alternating pattern between attractive and repulsive long-range interactions — predominantly sign-changing but occasionally allowing consecutive same-sign interactions, an effect that is further amplified by the interaction strength Δ . This means that, for instance, when two particles are separated by a distance r , they experience an attractive interaction, tending to reduce their separation to $r - 1$; however, at distance $r - 1$, the interaction becomes repulsive, pushing them back toward r . As a result, when interactions dominate, the inter-particle distance r tends to be maintained.

When Δ/J is sufficiently large such that interactions dominate, from an energy perspective, this sign-alternating interaction creates a significant energy difference, $\Delta E_1 = |E_{r+1} - E_r|$, between configurations whose inter-particle distances r differ by one lattice unit, further suppressing deviations from the initial separation. From exact diagonalization(ED) calculations, it is revealed that the system's eigenstates $|\phi_n\rangle$, defined by the eigenvalue equation

$$\hat{H}|\phi_n\rangle = E_n|\phi_n\rangle, \quad (6)$$

are predominantly composed of configurations with a fixed inter-particle distance. Consequently, when the system is initialized in a specific state $|\Psi(0)\rangle$ (e.g., particles at sites i_0 and j_0), the initial state typically projects dominantly onto a single eigenstate $|\phi_k\rangle$, with the corresponding weight $|c_k|^2 = |\langle\phi_k|\Psi(0)\rangle|^2$ being significantly larger than those of other eigenstates. Corresponding to the discussion above, however, occasionally the projection is shared comparably between two eigenstates, each carrying a substantial fraction of the total weight.

Next, we set $J = 1$ and $\Delta = 10$ ($\Delta/J=10$), such that the system energy is dominated by the interaction U , with the difference between the interaction energy U and the total energy E being on the order of 10^{-4} . Therefore, for simplicity in the following discussion—except in precise numerical fitting—the interaction energy U is used as the basis for energy comparison.

By tuning the phase φ , this phenomenon takes on three distinct manifestations: localization, nearest-neighbor separation oscillations, and next-nearest-neighbor separation transitions—each arising for specific initial separations r_0 .

Firstly, as shown in Fig. 3, the evolution of the probability density distribution in Eq. (2) reveals that, as φ is tuned, the two particles exhibit long-time localization when they start from one or more specific initial distances. This occurs because at these distances, the interaction U approaches zero. We consider a lattice of size $L = 23$ and an evolution time $t = 50$. Figs. 3(a) and (b) show that for $\varphi = 3\pi/8$, the two particles remain localized when the initial distance is 9, regardless of whether they initially lie on the boundary. Figs. 3(c)–(f) demonstrate that for $\varphi = \pi/64$, there are two initial distances leading to localization: 2 and 19. Notably, at distance 19 the interaction U is closer to zero, resulting in stronger localization. Moreover, from Figs. 3(c) and (d) it can be seen that, under the same conditions, localization is stronger when the particles are initially placed at the boundary than when both are in the interior.

Secondly, as the inter-particle distance changes by one lattice unit, the quasiperiodically modulated interaction is predominantly sign-changing, meaning that adjacent distances typically experience opposite signs (one attractive, one repulsive). Under this typical condition, the inter-particle distance remains conserved during the

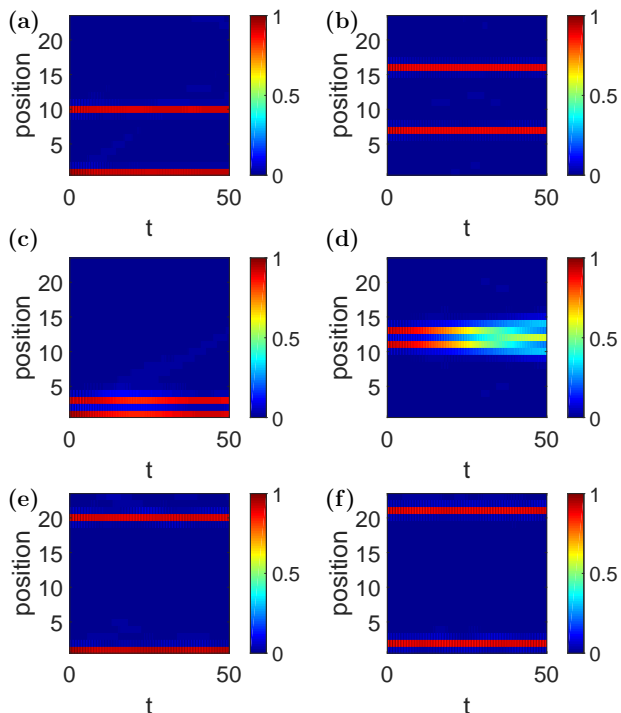


FIG. 3. Localization dynamics of two particles. The left (right) column shows initial configurations with one (neither) particle at the boundary. (a,b) For phase $\varphi = 3\pi/8$ and initial separation 9. (c–f) For the fixed phase $\varphi = \pi/64$, with two distinct initial separations: (c,d) separation = 2; (e,f) separation = 19. $L = 23$, $\Delta = 10$.

walk. However, occasionally the interaction yields consecutive same-sign interactions, where two distances differing by one site are either both attractive or both repulsive. In these exceptional cases, the two-particle distance oscillates between these two values, leading to a deviation from strictly conserved walk.

To observe this oscillation more clearly, independent of particle walk, we consider the case where both particles are initially placed at the boundaries (so that the initial separation equals the lattice length). While this configuration typically results in boundary localization, under specific conditions it instead reveals the oscillatory dynamics of interest; see Fig. 4.

The evolution of the probability density in Fig. 4(a) intuitively illustrates this oscillation. The Loschmidt echo (also known as the quantum return probability for pure states) [20] in Fig. 4(b) is defined as

$$L(t) = \left| \langle \Psi(0) | e^{-i\hat{H}t} | \Psi(0) \rangle \right|^2, \quad (7)$$

which quantifies the similarity between the time-evolved state and the initial state throughout the quantum dynamics. That is, the Loschmidt echo equals one at the initial time (when the state is identical to the initial state) and becomes zero when the state is completely

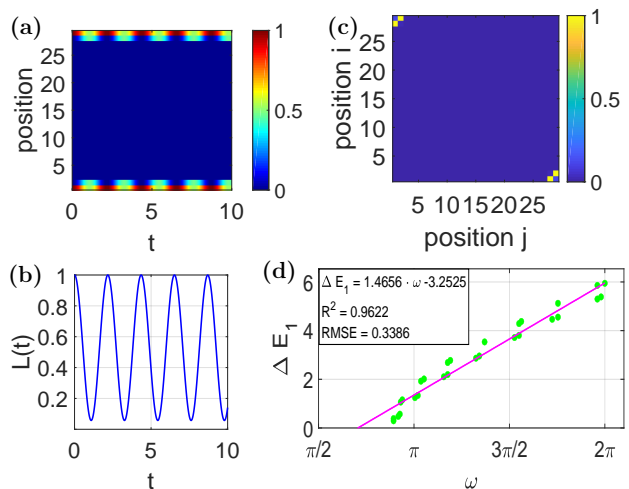


FIG. 4. Nearest-neighbor separation oscillations at the boundaries. Evolution of (a) the probability density distribution and (b) the Loschmidt echo [defined in Eq. (7)] up to $t = 10$. (c) Correlation function at $t = 1.09$, the moment when the Loschmidt echo $L(t)$ reaches its minimum. $L = 29$, $\Delta = 10$, $\varphi = 0$. (d) Angular frequency ω of the Loschmidt echo oscillation versus ΔE_1 . The 28 data points are selected from lattices of size $L = 8-71$ with $\Delta = 10$, $\varphi = 0$ or $\pi/2$, where oscillations are pronounced ($\omega \in (0, 2\pi]$).

different from the initial one. Fig. 4(c) shows the two-particle correlation function at the moment when the Loschmidt echo reaches its minimum ($t = 1.09$), indicating that the inter-particle distance is most likely one lattice unit less than the initial separation (the lattice length). Based on Eq. (6), we derive Eq. (7) as:

$$L(t) = \sum_n p_n^2 + 2 \sum_{n < m} p_n p_m \cos((E_n - E_m)t). \quad (8)$$

Here, $p_n = |c_n|^2$, satisfying the normalization condition $\sum_n p_n = 1$. It can be seen that the oscillatory terms in the time evolution are composed of a superposition of cosine functions. That is, if there are only two eigenstates in the system, the angular frequency ω of L is precisely the difference between the corresponding eigenenergies:

$$\omega_{nm} = E_n - E_m \quad (\text{in natural units } \hbar = 1). \quad (9)$$

However, as mentioned earlier, given that the initial state is not an exact eigenstate, and the system behavior may be more complex than that of an ideal two-level model, we cannot directly apply the simple form of Eq. (9). Instead, if we assume that the system dynamics are still governed by a pair of dominant eigenstates—each corresponding to a fixed inter particle distance—and that the energy difference ΔE_1 between them (as defined above) varies approximately linearly with the observed angular frequency of the Loschmidt echo ω , we can phenomenologically propose a linear relation:

$$\Delta E_1 = a \cdot \omega + b,$$

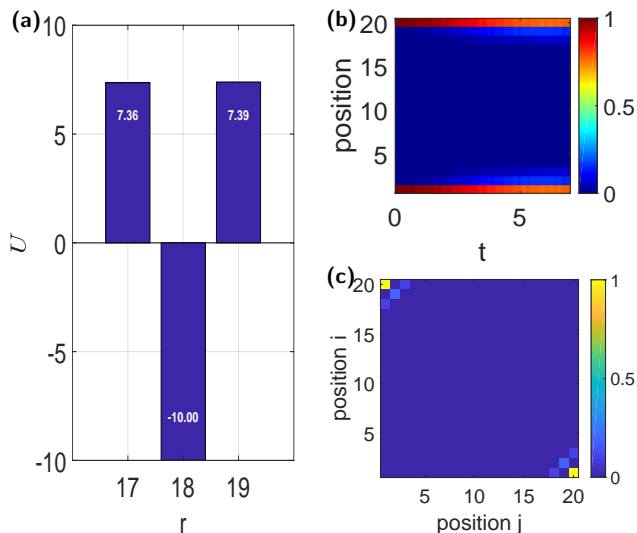


FIG. 5. Next-nearest-neighbor separation transitions. (a) Interaction energies for initial separations of 17, 18, and 19. (b) Time evolution of the probability density (two particles initially at boundaries) up to $t = 7$. (c) Correlation function at $t = 7$. $L = 20$, $\Delta = 10$, $\varphi = 3\pi/4$.

where a and b are fitting parameters. To test this hypothesis, we select 28 sample data points from lattices of size $L = 8$ to 71 by tuning the phase ($\varphi = 0$ or $\pi/2$), focusing on cases where boundary oscillations are pronounced. As shown in Fig. 4(d), we then fit ω against ΔE_1 using the least squares method, yielding an excellent linear fit:

$$\Delta E_1 = 1.4656\omega - 3.2525,$$

with a coefficient of determination $R^2 = 0.9622$ and a root-mean-square error $\text{RMSE} = 0.3386$.

Thirdly, by precisely tuning the phase φ , we can always find cases where the interaction signs are opposite for particle separations r differing by one lattice unit, while the interaction energies U are nearly equal for separations r differing by two lattice units, i.e., $U(r) \approx U(r+2)$, as shown in Fig. 5(a). For phase $\varphi = 3\pi/4$, consider separations r differing by one lattice unit—specifically, between $r = 18$ and $r+1 = 19$: $U(18) = -10$ and $U(19) = 7.39$, resulting in a large energy difference $\Delta E_1 \approx |U(19) - U(18)| = 17.39$. Such a significant energy barrier would normally keep the two particles moving at a constant distance. However, for separations differing by two lattice units, e.g., $r = 17$ and $r = 19$, the interaction energies are $U(17) = 7.36$ and $U(19) = 7.39$, respectively. The resulting energy difference $\Delta E_2 = |E_{r+2} - E_r| \approx |U(19) - U(17)| = 0.03$ is negligibly small, indicating near energy equality.

In this scenario, next-nearest-neighbor separation transitions occur with a small but finite probability: while the particles maintain an approximately constant separation, there remains a chance that the separation changes by two lattice units, as illustrated in Figs. 5(b)

and (c). Here, the two particles start at the boundaries of a lattice of length 20, with an initial separation $r_0 = 19$. Fig. 5(b) shows the time evolution of the probability density up to $t = 7$, and Fig. 5(c) displays the two-particle correlation function at $t = 7$. It can be seen that, starting from $r_0 = 19$, there is a finite probability that the separation transitions to $r = 17$ during evolution. This indicates that while the large energy difference for separations differing by one lattice unit ΔE_1 plays a major role in maintaining an approximately constant inter-particle distance under strong quasiperiodic interactions, the energy difference for separations differing by two lattice units ΔE_2 also plays a role.

Finally, we discuss the entanglement entropy of the system. For a two-particle system, the entanglement entropy is defined as the von Neumann entropy of the single-particle reduced density matrix $\rho_1(t)$ [21]:

$$S_1(t) = -\text{Tr}[\rho_1(t) \log_2 \rho_1(t)], \quad (10)$$

where the matrix elements of the single-particle reduced density matrix are given by:

$$[\rho_1(t)]_{x,x'} = \langle \Psi(t) | \hat{c}_x^\dagger \hat{c}_{x'} | \Psi(t) \rangle, \quad (11)$$

with $x, x' = 1, 2, \dots, L$ labeling the lattice sites, and $|\Psi(t)\rangle$ being the two-particle state vector (consistent with the definitions in Eqs. (2) and (3)).

For our system with $L = 23$ lattice sites (see Figs. 6(a)–(d) and (f)) and $L = 29$ lattice sites (see Fig. 6(e)), the theoretical maximum of the single-particle reduced von Neumann entropy is $\log_2 23 \approx 4.52$ and $\log_2 29 \approx 4.85$, respectively, which are attained only when the reduced density matrix is maximally mixed. In contrast, we identify a clear suppression of entanglement entropy in all panels of Fig. 6.

Comparing Figs. 6(a) and 6(b), we observe that the suppression of entanglement entropy is more pronounced for larger particle separations—as seen in Fig. 6(b). Figs. 6(c) and (d) correspond to Figs. 3(c) and (e), respectively, indicating that in the localized regime, the entanglement entropy remains relatively stable over long times. A higher degree of localization (e.g., Fig. 3(e)) corresponds to lower entanglement entropy, and vice versa. Fig. 6(e) illustrates the second manifestation discussed earlier, where the two particles start at the boundaries and exhibit oscillatory behavior. In this scenario, the entanglement entropy also oscillates, taking values between 1 and 2, consistent with the oscillatory behavior of $L(t)$ (i.e., the same frequency but different amplitude) in Fig. 4(b). Fig. 6(f) shows the entanglement entropy in a special case where the inter-particle distance oscillates while maintaining constant-distance walk. This oscillation of the entanglement entropy is also consistent with the oscillatory behavior of $L(t)$ in the same case. Here, with $L = 23$ and initial positions (1, 21), the entanglement entropy exhibits an unusual oscillatory pattern.

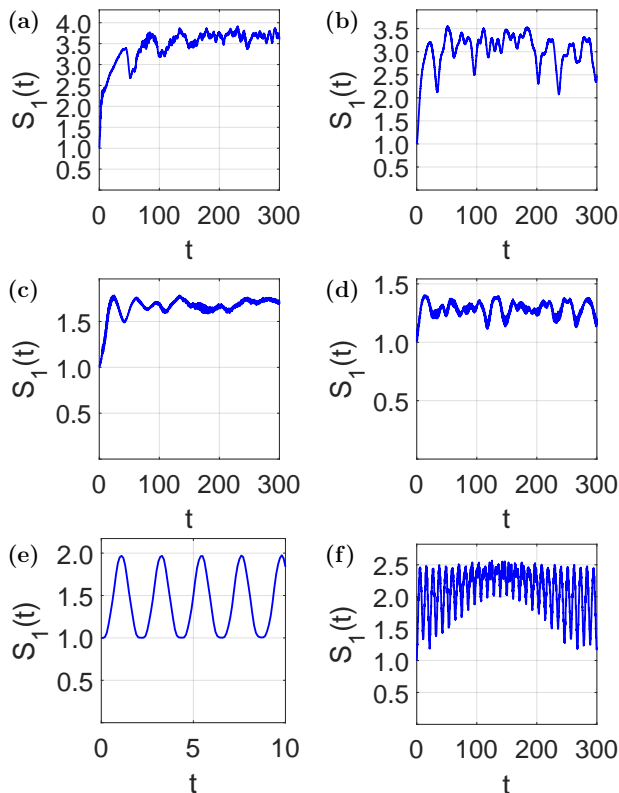


FIG. 6. Entanglement entropy [defined in Eq. (10)] for the approximate constant-distance walking regime. (a) Initial separation 3 and (b) initial separation 17, with $L = 23$, $\Delta = 10$, $\varphi = 0$, $t = 300$. (c) Initial separation 2 (cf. Fig. 3(c)) and (d) initial separation 19 (cf. Fig. 3(e)), with $L = 23$, $\Delta = 10$, $\varphi = \pi/64$, $t = 300$. (e) Oscillation at the boundary; $L = 29$, $\Delta = 10$, $\varphi = 0$, $t = 10$. (f) Initial positions (1, 21); same parameters as in (a).

In summary, we have observed a phenomenon of approximately constant-distance walk for two particles in a one-dimensional lattice under strong quasiperiodic long-range interactions. Among the three manifestations we have focused on, localization—where the interparticle distance remains fixed—represents a special form of this constant-distance walk. The other two manifestations, namely nearest-neighbor separation oscillations and next-nearest-neighbor separation transitions, account for the approximate nature of the walk: the former occurs more commonly under a wide range of parameters, while the latter emerges only under a narrow range of conditions. Although our study of the two-particle case is limited to OBC and fermions, the underlying mechanism suggests that this phenomenon can also appear in infinite chains and for hard-core bosons. Our work extends the understanding of dynamics in few-body models with long-range interactions and quasiperiodic elements. Furthermore, the investigation of entanglement entropy in various scenarios of this model may advance related fields in quantum information. Our findings open up

the possibility of studying similar long-range lattice models. Future directions of interest include the modulation of the spatial frequency of the quasiperiodic interactions and its effect on these phenomena, as well as investigations involving more than two particles.

* 12024117009@stu.ynu.edu.cn

- [1] A. Polkovnikov, K. Sengupta, A. Silva, and M. Vengalattore, *Reviews of Modern Physics* **83**, 863 (2011).
- [2] J. Eisert, M. Friesdorf, and C. Gogolin, *Nature Physics* **11**, 124 (2015).
- [3] N. Defenu, T. Donner, T. Macrì, G. Pagano, S. Ruffo, and A. Trombettoni, *Reviews of Modern Physics* **95**, 035002 (2023).
- [4] M. Saffman, T. G. Walker, and K. Mølmer, *Reviews of modern physics* **82**, 2313 (2010).
- [5] L. Chomaz, I. Ferrier-Barbut, F. Ferlaino, B. Laburthe-Tolra, B. L. Lev, and T. Pfau, *Reports on Progress in Physics* **86**, 026401 (2022).
- [6] L. D. Carr, D. DeMille, R. V. Krems, and J. Ye, *New Journal of Physics* **11**, 055049 (2009).
- [7] C. Monroe, W. C. Campbell, L.-M. Duan, Z.-X. Gong, A. V. Gorshkov, P. W. Hess, R. Islam, K. Kim, N. M. Linke, G. Pagano, *et al.*, *Reviews of Modern Physics* **93**, 025001 (2021).
- [8] H. Ritsch, P. Domokos, F. Brennecke, and T. Esslinger, *Reviews of Modern Physics* **85**, 553 (2013).
- [9] F. Mivehvar, F. Piazza, T. Donner, and H. Ritsch, *Advances in Physics* **70**, 1 (2021).
- [10] Z. Wu, J. Fan, X. Zhang, J. Qi, and H. Wu, *Physical Review Letters* **131**, 243401 (2023).
- [11] T. D. Ladd, F. Jelezko, R. Laflamme, Y. Nakamura, C. Monroe, and J. L. O'Brien, *nature* **464**, 45 (2010).
- [12] S. Aubry and G. André, *Ann. Israel Phys. Soc* **3**, 18 (1980).
- [13] M. Schreiber, S. S. Hodgman, P. Bordia, H. P. Lüschen, M. H. Fischer, R. Vosk, E. Altman, U. Schneider, and I. Bloch, *Science* **349**, 842 (2015).
- [14] Z. Tao, W. Huang, J. Niu, L. Zhang, Y. Ke, X. Gu, L. Lin, J. Qiu, X. Sun, X. Yang, *et al.*, arXiv preprint arXiv:2303.04582 (2023).
- [15] T. Nicholson, S. Blatt, B. Bloom, J. Williams, J. Thomsen, J. Ye, and P. S. Julienne, *Physical Review A* **92**, 022709 (2015).
- [16] L. W. Clark, L.-C. Ha, C.-Y. Xu, and C. Chin, *Physical review letters* **115**, 155301 (2015).
- [17] Z. Guo and Z. Cai, *Physical Review B* **111**, 134202 (2025).
- [18] Y. Lahini, M. Verbin, S. D. Huber, Y. Bromberg, R. Pugatch, and Y. Silberberg, *Physical Review A—Atomic, Molecular, and Optical Physics* **86**, 011603 (2012).
- [19] L. Wang, N. Liu, S. Chen, and Y. Zhang, *Physical Review A* **92**, 053606 (2015).
- [20] P. L. Krapivsky, J.-M. Luck, and K. Mallick, *Journal of Statistical Mechanics: Theory and Experiment* **2018**, 023104 (2018).
- [21] W.-H. Zhong, H.-Q. Lin, and X.-J. Yu, *Physical Review B* **112**, 075129 (2025).